Evaluation of metabolomic changes during neoadjuvant chemotherapy combined with bevacizumab in breast cancer using MR spectroscopy

Leslie R. Euceda[1], Tonje H. Haukaas[1,2], Guro F. Giskeødegård[1,3], Riyas Vettukattil[1], Jasper Engel[4], Laxmi Silwal-Pandit[2,5], Steinar Lundgren[6,7], Elin Borgen[2,8], Øystein Garred[2,8], Geert Postma[9], Lutgarde M.C. Buydens[9], Anne-Lise Børresen-Dale[2,5], Olav Engebraaten[2,10], Tone F. Bathen[1,2]

[1]Department of Circulation and Medical Imaging, Faculty of Medicine and Health Sciences, NTNU - Norwegian University of Science and Technology, Trondheim, Norway

[2]K.G. Jebsen Center for Breast Cancer Research, Institute of Clinical Medicine, University of Oslo, Oslo, Norway

[3]St. Olavs Hospital, Trondheim University Hospital, Trondheim, Norway

[4]NERC Biomolecular Analysis Facility Metabolomics Node (NBAF-B), School of Biosciences, University of Birmingham, Birmingham, UK

[5]Department of Cancer Genetics, Institute for Cancer Research, Oslo University Hospital, The Norwegian Radium Hospital, Oslo, Norway

[6]Department of Cancer Research and Molecular Medicine, Faculty of Medicine and Health Sciences, NTNU - Norwegian University of Science and Technology, Trondheim, Norway

[7]Cancer Clinic, St. Olavs Hospital, Trondheim University Hospital, Trondheim, Norway

[8]Department of Pathology, Division of Diagnostics and Intervention, Oslo University Hospital, Oslo, Norway

[9]Institute for Molecules and Materials, Radboud University Nijmegen, Nijmegen, The Netherlands

[10]Department of Oncology and Department of Tumor Biology, Oslo University Hospital, and Department of Clinical Medicine, University of Oslo, Norway

Published in: Metabolomics, 2017; 13:37
https://link.springer.com/article/10.1007/s11306-017-1168-0

Corresponding author: Leslie R. Euceda, Department of Circulation and Medical Imaging - MR Center, Faculty of Medicine and Health Sciences, NTNU - Norwegian University of Science and Technology, Postboks 8905, Medisinsk Teknisk Forskningssenter, 7491 Trondheim, Norway; Phone: +47 73597449, Fax: +47 73598613, E.mail: leslie.e.wood@ntnu.no.

Acknowledgements: The authors would like to thank Øyvind Salvesen for useful discussions regarding linear mixed-effects models and Santosh Lamichhane for technical support during HR MAS MRS acquisition. The HR MAS MRS analysis was performed at the MR Core Facility, Norwegian University of Science and Technology (NTNU), which is funded by the Faculty of Medicine at NTNU and Central Norway Regional Health Authority.

The study was funded in part by generous grants from:

(1) The Research Council of Norway, Imaging the breast cancer metabolome, Project no 221879
(2) The Pink Ribbon Movement and Norwegian Breast Cancer Society
(3) K. G. Jebsen Center for Breast Cancer Research
(4) Roche Norway
(5) Sanofi-Aventis Norway

Abstract

Introduction: Metabolomics investigates biochemical processes directly, potentially complementing transcriptomics and proteomics in providing insight into treatment outcome.

Objectives: This study aimed to use magnetic resonance (MR) spectroscopy on breast tumor tissue to explore the effect of neoadjuvant therapy on metabolic profiles, determine metabolic effects of the antiangiogenic drug bevacizumab, and investigate metabolic differences between responders and non-responders.

Methods: Breast tumors from 122 patients were profiled using high resolution magic angle spinning MR spectroscopy. All patients received neoadjuvant chemotherapy, and were randomized to receive bevacizumab or not. Tumors were biopsied prior, during, and after treatment.

Results: Principal component analysis showed clear metabolic changes indicating a decline in glucose consumption and a transition to normal breast adipose tissue as an effect of chemotherapy. Partial least squares-discriminant analysis revealed metabolic differences between pathological minimal residual disease patients and pathological non-responders after treatment (accuracy of 77%, $p<0.001$), but not before or during treatment. Lower glucose and higher lactate was observed in patients exhibiting a good response (≥90% tumor reduction) compared to those with no response (≤10% tumor reduction) before treatment, while the opposite was observed after treatment. Bevacizumab-receiving and chemotherapy-only patients could not be discriminated at any time point. Linear mixed-effects models revealed a significant interaction between *time* and *bevacizumab* for glutathione, indicating higher levels of this antioxidant in chemotherapy-only patients than in bevacizumab receivers after treatment.

Conclusion: MR spectroscopy showed potential in detecting metabolic response to treatment and complementing other molecular assays for the elucidation of underlying mechanisms affecting pathological response.

Keywords: bevacizumab, breast cancer, chemotherapy, HR MAS MRS, metabolomics, neoadjuvant

INTRODUCTION

Breast cancer prognosis has improved during the past decades (Ferlay et al. 2013), attributed to earlier detection through effective mammography screening and improved therapy (American Cancer Society 2011; Malmgren et al. 2014; Giordano et al. 2004). However, with the disease still being the leading cause of cancer death in women (Ferlay et al. 2013; American Cancer Society 2011), defining new tools to stratify patients to targeted therapy and to detect early response is warranted.

Neoadjuvant or preoperative therapy is used to treat locally advanced breast tumors where size is too large for surgical mastectomy with acceptable margins or to allow for breast conserving surgery (Miller et al. 2014). The effect of neoadjuvant treatment on progression-free survival (PFS) and overall survival (OS) is comparable to adjuvant or post-operative therapy (van der Hage et al. 2001), enabling the possibility for molecular analyses on tumor samples before, during, and after therapy, and a direct visualization of the treatment effect by pathological examination after removal of the tumor.

Angiogenesis, the formation of new blood vessels from existing vasculature, is a hallmark of cancer needed for the supply of nutrients and oxygen to the tumor (Hanahan and Weinberg 2000) and may be therapeutically targeted. Vascular endothelial growth factor (VEGF), a proangiogenic factor, can be inhibited by bevacizumab, a humanized monoclonal antibody (Ferrara et al. 2004). Addition of neoadjuvant bevacizumab to chemotherapy has resulted in better responses or increase in PFS, but has not increased OS (Miller et al. 2007). As for all targeted anticancer agents used in breast cancer, a reliable marker for the selection of patients who benefit from antiangiogenic therapy is needed.

Much of the variability in breast cancer treatment response has been attributed to tumor heterogeneity (Ng et al. 2012). Breast cancer has been divided into five molecular subtypes based on gene expression patterns found to have significant differences in clinical outcome (Perou et al. 2000; Sørlie et al. 2003). Metabolites are downstream of gene expression in the biochemical information flow known as the omics cascade, and altered metabolism is an emerging hallmark of cancer (Hanahan and Weinberg 2011). High resolution (HR) magic angle spinning (MAS) magnetic resonance spectroscopy (MRS) of intact tissue has been applied to study metabolites involved in important pathways in different cancers (Moestue et al. 2011; Bathen et al. 2010) . HR MAS MRS has been employed to relate metabolic changes after treatment to 5-year survival in breast cancer patients receiving neoadjuvant single agent chemotherapy followed by endocrine adjuvant therapy (Cao et al. 2012) and to reveal variability in metabolic profiles of breast tumors within the same gene-expression subtype (Borgan et al. 2010; Haukaas et al. 2016). Thus, MR metabolomics can provide complimentary insight into breast cancer treatment outcome. This study aimed to use MRS to explore the metabolic changes in breast tumor tissue occurring as an effect of overall neoadjuvant therapy, to investigate metabolic differences between therapy responders and non-responders, and to determine the metabolic effects of antiangiogenic treatment with bevacizumab. Particular focus was given to

metabolites involved in the pathways of glycolysis, choline phospholipid metabolism, and glutaminolysis, due to their high relevance for cancer.

METHODS

Patient and tumor characteristics

Tumor tissue from 122 breast cancer patients included in the NeoAva study, a phase 2 randomized clinical trial, were examined. Women (age ≥ 18 years) with large (size ≥ 2.5 cm), non-metastatic, human epidermal growth factor receptor 2 (HER2) negative tumors were recruited in the period of November 2008 – July 2012. All patients received neoadjuvant chemotherapy in the form of FEC100 (5-fluorouracil 600 mg/m2, epirubicin 100 mg/m2, cyclophosphamide 600 mg/m2) followed by taxane-based therapy, while they were randomized to receive bevacizumab or not (See Online Resource 1). Ultrasound-guided needle biopsies were sampled prior to treatment (TP1) and 12 weeks into treatment (TP2), while biopsies at 24 weeks (TP3) were obtained from the surgically removed tumor. For details on sample handling, see Online Resource 1. The study was registered in the http://www.ClinicalTrials.gov/ database with the identifier NCT00773695. Patient and tumor characteristics are shown in Table 1, and the study design is illustrated in Fig. S1 (Online Resource 2).

Evaluation of treatment response

Analysis of only cases with pathological complete response (pCR) (20/122 patients) would result in a loss of information from the patients experiencing a good response, but not achieving pCR (44/122). Therefore, in addition to the pCR endpoint, we introduced a cut-off value of 1 cm for the tumor diameter measured pathologically at the time of surgery (TP3) to classify patients as having pathological minimal residual disease (pMRD) or as pathological non-responders (pNRs) (diameter <1cm and >1cm, respectively). Furthermore, a 'response ratio' inversely proportional to tumor reduction was calculated as: tumor diameter at TP3/tumor diameter at TP1. Response ratio >1 indicates an increase in tumor size with treatment. At TP1, the diameter was measured using magnetic resonance imaging (MRI). For patients with no available MRI measurement at TP1 (21/122 patients), the maximum value from ultrasound and/or mammography-measured diameters was used. Patients were categorized as having good, intermediate, or no response (GR, IR, NR) based on response ratio (≤0.10, >0.10 - <0.90, or ≥0.90, respectively).

Gene expression subtyping

Gene expression microarray data was acquired and processed as described in Online Resource 1. The PAM50 algorithm (Parker et al. 2009) was used to classify samples by gene expression subtype. Gene expression microarray data is available in the ArrayExpress database (http://www.ebi.ac.uk/arrayexpress) under accession number E-MTAB-4439.

HR MAS MRS Experiments and Data preprocessing

Tissue samples (4.1 ± 1.3 mg) were analyzed by HR MAS MRS in accordance with (Giskeødegård et al. 2015) as described in Online Resource 1.Sample availability at each time point varied for each patient (n=325 total analyzed samples). Samples with high lipid content (n=23) and giving spectra of poor quality, i.e. poor shimming and insufficient water suppression (n=17), were excluded. Additionally, fifteen samples collected from patients with tumors not evaluable for pathological measurement of diameter at TP3 were excluded, resulting in 270 samples for subsequent statistical analysis. Preprocessing before selection of spectral regions for further analysis was carried out in Matlab R2013b (The Mathworks, Inc., USA) as described in Online Resource 1. Lipid peaks at 4.37-4.27, 2.97-2.70, 2.31-2.23, 2.11-1.92, 1.64-1.49 ppm, and the contaminant peaks for ethanol and acetone at 3.71-3.63 and 2.23-2.21 ppm, respectively, were excluded. Regions containing peaks from lidocaine, a local anesthetic used for sampling biopsies at TP1 and TP2, at 3.38-3.30 and 2.21-2.17 ppm, were also excluded. The spectra were subsequently PQN (Dieterle et al. 2006) normalized. Normalization after lipid removal corrects for differences in sample size and tumor cell content, as it can be assumed that the majority of the lipid signals arise from normal adipose cells within the tumor specimen obtained.

Statistical analysis

Multivariate analyses

Multivariate analysis was carried out in Matlab R2013b (The Mathworks, Inc., USA) using PLS Toolbox 7.8.2 (Eigenvector Research Inc., U.S.A). Spectra were mean-centered prior to multivariate modelling. Principal component analysis (PCA) (Wold et al. 1987) was employed using residual explained variance plots to select the number of principal components (PCs). Partial least squares-discriminant analysis (PLS-DA) (Wold et al. 2001) models were built for each separate time point to discriminate between pCR+ and pCR-, pMRD and pNR, the two extreme response ratio groups of GR and NR, bevacizumab-treated and chemotherapy-only patients, and bevacizumab-treated pMRD and chemotherapy-only pMRD. PLS-DA models were validated using double-layered cross validation (CV) (Westerhuis et al. 2008) for separate latent variable (LV) number optimization and classification assessment, to avoid overfitting. Furthermore, permutation testing (Westerhuis et al. 2008) was employed to evaluate model statistical significance. Model validation is detailed in Online Resource 1. For PLS-DA plots, y-variance was condensed into the first LV through orthogonal-PLS (OPLS) (Eigenvector Research 2013) when the number of optimal LVs >1.

Univariate analyses

Metabolites were assigned based on previous identification (Sitter et al. 2002) and relative levels were calculated by integrating fixed regions of preprocessed spectra (prior to normalization) corresponding to each metabolite in Matlab R2013b. The integrals were then subsequently PQN normalized to correct for differences in sample weight. The integral of the metabolite lactate (Lac) was not calculable in 116 samples due to presence of an overlapping peak originating from the C_1H_2 of the glycerol backbone of phospholipids and triglycerides at 4.13 ppm. For these samples, the Lac levels were imputed in R 3.1.1 (R Core Team 2014) using the package for the method of multivariate imputation by chained equations (MICE) (van Buuren and Groothuis-Oudshoorn 2011) set to predictive mean matching and 10 imputations (Rubin 1987). This procedure was validated as described in Online Resource 1. All metabolite integrals were log10 transformed before univariate tests were conducted to satisfy prerequisite assumptions of normality (Matlab R2013b). Student's t-tests were conducted to compare metabolite levels between different groups. Pearson correlations between metabolite relative levels and response ratio for each separate time point were calculated in SPSS Statistics 22.0, (IBM Corp., U.S.A.).

Linear mixed-effects models (LMM) (Pinheiro and Bates 2000) for individual metabolite multilevel analysis of data grouped according to different classification factors were built in R 3.1.1 using the function *lme* from the 'nlme' package (Pinheiro et al. 2014) employing the method of restricted maximum likelihood. LMM describe relationships between a response variable and these factors incorporating two types of effects: fixed which are controlled and random which depend on each individual. Here, the response variable was the metabolite level while the fixed effects were *time* (TP1, TP2, or TP3), *pMRD response* (pMRD or pNR), and *bevacizumab* (bevacizumab-treated or chemotherapy-only) and the random effect was the patient ID. Significance of interactions between fixed effects was evaluated as described in Online Resource 1. Visual inspection of residual q-q plots and histograms did not reveal obvious deviations from normality.

Multiple testing correction of the p-values resulting from Pearson correlations and LMM was performed by the Benjamini Hochberg method for false discovery rate (FDR) adjustment in R 3.1.1 using the 'stats' package (R Core Team 2014). Statistical significance was considered for adjusted p (q-value) ≤ 0.05.

RESULTS

Metabolic effects of neoadjuvant chemotherapy

The sample composition of the cohort according to gene expression subtype, time point, pMRD response group, and bevacizumab randomization group is summarized in Fig. S2 in Online Resource 2. PCA was employed on all spectra to investigate trends in the sample cohort as a whole (Fig. 1).

Clear changes in metabolic profiles were observed with time (Fig. 1A). The scores plot labeled by gene-expression subtype (Fig. 1C) revealed a separation of the metabolic profiles of normal-like subtype samples from the rest. Comparing Fig. 1A and Fig. 1C, most TP3 samples were of the normal-like gene expression subtype, also observed in Fig. S2F (Online Resource 2). The loadings plot (Fig. 1D) clearly indicated elevated phosphocholine (PCh), glycerophosphocholine (GPC), and taurine (Tau) at TP1, while glucose (Glc) and lipids were higher with increasing time of treatment and in normal-like samples.

Sixteen metabolites were identified as measurable, and their relative intensities were calculated by peak integration and log10 transformed. The metabolite data is available in Online Resource 3.

LMM revealed significant differences after multiple testing correction in 11/16 metabolites for the factor *time* (Table 2), including the metabolites detected in PCA with the exception of Tau. Four out of these 11 metabolites were significantly different for TP2 vs TP1, while all 11 of them were significant for TP3 vs TP2. Seven metabolites exhibited a significant interaction between *time* and *pMRD response*, while a significant interaction between *time* and *bevacizumab* was detected only for glutathione (GSH) (Supplementary Table 3 in Online Resource 4).

Metabolic differences between responders and non-responders

Results from PLS-DA discrimination of patients at each time point based on three different response criteria using metabolic profiles are summarized in Supplementary Table 4 in Online Resource 4. Metabolic differences between pCR+ and pCR- were detected at TP3 (Fig. 2A), but not TP1 or TP2, with an accuracy of 69% ($p=0.018$). Similarly, a significant discrimination between pMRD and pNRs was achieved only at TP3 (Fig. 2C), with PLS-DA model performance improving greatly (accuracy=77%, $p<0.001$). Compared to pCR- and pNR, both pCR+ and pMRD, respectively, showed elevated Glc and Lac and decreased creatine (Cr), glycine (Gly), Tau, GPC, PCh, choline (Cho), succinate (Succ), and alanine (Ala) levels (Fig. 2B, Fig. 2D).

PLS-DA significantly discriminated spectra from patients in the extreme response ratio groups of GR and NR at TP1 and TP3, but not TP2, with an accuracy of 76% ($p=0.001$) and 75% ($p=0.002$), respectively. The GR group showed lower levels of Glc and higher levels of ascorbate (Asc), Lac, Tyr, Cr, Gly, Tau, GPC, PCh, Cho, GSH, Succ, glutamate (Glu), and Ala compared to the NR group at TP1 (Fig. 3A-3B), while the opposite was observed at TP3 (Fig. 3C-3D). In addition, relative levels of two and eight metabolites were significantly correlated with the response ratio at TP1 and TP3, respectively (Supplementary Table 5 in Online Resource 4, Fig. S3 in Online Resource 2), but not at TP2. A switch in the direction of the correlation trend (positive or negative) was observed in the two metabolites with significant correlations at both time points (Glc and Tau).

Applying the multilevel approach of LMM, Lac was the only significant metabolite for the factor *pMRD response* (Table 2). However, the interaction between *time* and *pMRD response* was significant for seven metabolites (Supplementary Table 3 in Online Resource 4), indicating that the effect of the *pMRD response* factor varies at different time points. *pMRD response* was significant at TP2 for Glc, Tyr, and Succ, while all seven metabolites were significant for this factor at TP3.

The most relevant results pertinent to treatment effect and comparison between responders and non-responders are summarized by pathway in Fig. 4, complemented by Supplementary Table 6 in Online Resource 4.

Glutathione metabolism identified as possibly affected by bevacizumab

PLS-DA could not discriminate bevacizumab-treated from chemotherapy-only patients at any time point. Both multivariate PLS-DA and univariate t-tests were employed to investigate differences between responding patients that were treated with additional bevacizumab and chemotherapy only. Significant metabolic differences between these groups could not be detected by either method at any time point (see Supplementary Table 7 and 8 in Online Resource 4).

For the multilevel LMM, *bevacizumab* was the only factor for which no metabolite was significant after multiple testing correction. However, a significant interaction between *time* and *bevacizumab* was detected for GSH (Table 2). GSH was significantly higher in controls than in bevacizumab-treated patients at TP3 ($p < 0.001$) (Supplementary Table 3 in Online Resource 4).

DISCUSSION

In this study we used MR based metabolic profiling of breast cancer tissue to investigate the effect of neoadjuvant chemotherapy in a large cohort of HER2 negative breast cancer patients randomized to receive additional bevacizumab treatment or not. The study design included three sampling time points over the treatment course, which allowed for a multilevel approach to investigate metabolic differences between patient groups.

Despite metabolic profiles not being able to predict pCR prior to treatment, a significant metabolic difference in pCR+ patients compared to pCR- was detected after neoadjuvant chemotherapy. This metabolic difference was even clearer when comparing pMRD patients and pNRs, with the former displaying similar metabolite trends as pCR+ patients. Moreover, a metabolic difference both before and after treatment was identified comparing patients with good response and no response. However, since the majority of cancer cells in pathological responders have responded to treatment, when comparing pMRD and pNRs at TP3, findings may also reflect metabolic differences between tumor and normal tissue. Previous studies using HR MAS MRS metabolic profiles of intact breast tumor

tissue have successfully identified patients with more than 5-year survival, while association to treatment response was more subtle (Cao et al. 2012; Cao et al. 2011). Findings from the NASBP B-40 trial report a significant increase in OS of HER2 negative breast cancer patients receiving chemotherapy with addition of neoadjuvant bevacizumab continued post-operatively (Bear et al. 2015). The significant discrimination of pathological response at surgery (TP3) based on metabolic profiles may be predictive of patients who would benefit from post-operative bevacizumab treatment. Metabolic signatures in patients with 5-year DFS, PFS and OS for this cohort will be investigated in due course.

Clear metabolic differences between time points in accordance with tumor reduction were observed. The increase in glucose with treatment progression points to a decline in glucose consumption, which is characteristically rapid in cancer cells, referred to as a glycolytic phenotype, to fulfill their high energy demands (Vander Heiden et al. 2009). Glucose was also found to be significantly higher in pMRD patients compared to pNRs after completion of neoadjuvant therapy, indicating an even greater decline in the consumption of glucose in the former group. The increase of lipids towards TP3 suggests a transition to normal breast adipose tissue. Lipid metabolism plays an important role in tumor cell apoptosis and necrosis resulting from treatment (Huang and Freter 2015). However, it can be assumed that most lipid signals arise from normal breast adipose cells. This is supported by samples at TP3 and of the normal-like subtype, which displays high expression of adipose cell genes (Perou et al. 2000), corresponding well in the PCA scores plot (Fig. 1A and 1C).

Metabolites that significantly decreased with treatment progression include glycerophosphocholine, phosphocholine, and choline, with the latter two also being significantly lower in pMRD patients compared to pNRs at TP3. These metabolites are involved in the metabolism of phosphatidylcholine, the most abundant phospholipid in eukaryote cell membranes (Gibellini and Smith 2010). Although the underlying mechanisms governing abnormal choline metabolism in cancer are still not fully understood (Glunde et al. 2011; Moestue et al. 2012), increase in the levels of choline containing metabolites are thought to be an indicator of malignant transformation and cancer aggressiveness (Aboagye and Bhujwalla 1999). Decreased phospholipid metabolism may be an indicator of a reduction in tumor malignancy and aggressiveness due to neoadjuvant chemotherapy. Further, studies showing that the behavior of choline metabolites varies between breast cancer subtypes (Giskeødegård et al. 2010; Grinde et al. 2014) indicate that the stratification of patients for treatment targeting phospholipid metabolism may be beneficial. This is further supported by our recent study (Haukaas et al. 2016) in which we used metabolic profiles to derive naturally-occurring metabolic subgroups, revealing that one of these contained significantly higher phosphocholine and glycerophosphocholine levels and less active degradation of phosphatidylcholine determined by integrative pathway analysis.

LMM additionally revealed increased glutamine with treatment progression indicating a decrease in glutaminolysis. The normally non-essential amino acid glutamine becomes an important alternative source of carbon and nitrogen for glucose-deprived cancer cells, replenishing the TCA cycle and providing substrates for nucleotide, lipid, and protein biosynthesis (Hensley et al. 2013). Glutamine is converted to glutamate, a precursor of non-essential amino acids and glutathione. Glutathione is a major cellular antioxidant which protects cancer cells against apoptosis caused by reactive oxygen species (ROS) (Franco and Cidlowski 2009). A significant interaction between *time* and *bevacizumab* was detected for glutathione, with chemotherapy-only patients exhibiting significantly higher levels than patients receiving bevacizumab at TP3. This is coherent with previously reported reduced levels of glutathione with bevacizumab treatment of glioblastoma (Fack et al. 2015). Bevacizumab may thus play a redox destabilizing role in cancer cells, inducing oxidative stress to promote apoptosis. It may therefore be interesting to monitor oxidative stress with bevacizumab treatment.

A significant LMM interaction between *time* and *response* was detected for succinate, showing significantly lower levels in pMRD patients compared to pNRs at TP2 and TP3. Succinate is the substrate of succinate dehydrogenase (SDH), a tricarboxylic acid (TCA) cycle enzyme which has been identified as a tumor suppressor (Selak et al. 2005). Inactivation of SDH leads to accumulation of succinate, which mediates signaling pathways promoting resistance to apoptotic signals and inhibits the degradation of HIF alpha, a transcription factor that promotes the glycolytic phenotype characteristic of cancer cells (King et al. 2006). Decreased succinate in responders, observed at both TP2 and TP3, is therefore in accordance with a less malignant phenotype.

Unexpectedly, a significant increase in lactate with treatment progression and in pMRD patients compared to pNRs was detected, similarly as for glucose. Both increased lactate production and rapid glucose consumption are characteristic of the Warburg effect, which is the metabolic switch from anaerobic to aerobic glycolysis observed in most cancer cells (Vander Heiden et al. 2009). Lactate has been associated with poor prognosis in ER positive breast cancer (Giskeødegård et al. 2012) as well as in other cancers (Saraswathy et al. 2009; Walenta and Mueller-Klieser 2004; Walenta et al. 2000). Still, the glycolytic phenotype is not absolute in cancer cells, as a better-oxygenated subpopulation uses lactate as the main energy source fueling oxidative phosphorylation (Hanahan and Weinberg 2011; Semenza 2008; Feron 2009). A dual metabolic effect in cancer cells has been suggested (Xie et al. 2014), where lactic acidosis, although a consequence of the Warburg effect, can convert the usually dominant Warburg effect to a non-glycolytic phenotype, decreasing glucose consumption. Elevated lactate promoting this non-glycolytic phenotype is a possible explanation for glucose and lactate not behaving oppositely as expected. Another possibility is that chemotherapy may produce morphological changes in tissue that impede adequate lactate cellular excretion, leading to its accumulation. An issue to be kept in mind is that imputation was employed to calculate the relative

levels of lactate for 116/270, which can be considered a limitation of this study. However, the imputation process was validated achieving a root mean square error (RMSE) of 0.006 and a coefficient of determination (R^2) of 0.9996, indicating high confidence for the predicted lactate values.

Regarding the multivariate comparison between good response and no response groups based on the response ratio, glucose and lactate behaved oppositely in both groups at both TP1 and TP3, contrary to them exhibiting trends in the same direction in pMRD patients and pNRs at TP3. However, when including samples from all three response ratio groups, glucose and lactate were both significantly negatively correlated with tumor size increase at TP3. The contradictory lactate/glucose behavior using different response criteria may therefore be due to the exclusion of 69/122 patients when comparing the two extreme response ratio groups. Lower glucose and higher lactate in the good response group before treatment points to a higher Warburg effect compared to the no response group, which is subsequently reversed in these groups by the end of treatment. In the same way, compounds associated with a more malignant phenotype including the choline containing metabolites, glutathione, glutamate, and succinate were elevated in the good response group before treatment, while the opposite was observed at the end of treatment. Although models built with these extreme groups cannot be used for prediction of treatment response, since a large part of the population has been excluded, these findings suggest that patients with a more malignant metabolic profile are more prone to benefit from treatment in terms of tumor reduction.

Changes in glutathione metabolism were identified as a possible effect of bevacizumab based on a significant interaction between *time* and *bevacizumab* using LMM for this metabolite. A substantial metabolic effect due to chemotherapy in both bevacizumab-treated and chemotherapy-only patients was evidenced, suggesting the potent chemotherapeutic effect may mask many of the effects of bevacizumab. In addition, the increase in lactate observed with increasing time on therapy may counteract VEGF inhibition by bevacizumab, as it has been found that excreted lactate from tumor cells stimulates angiogenesis dependent of a different proangiogenic factor: interleukin 8 (IL-8) (Végran et al. 2011). IL-8 signaling has been found to compensate for inhibition of VEGF-dependent angiogenesis in bevacizumab-resistant cells of head and neck squamous cell carcinoma (Gyanchandani et al. 2013). Altered lactate metabolism as a mechanism of bevacizumab resistance should therefore be further investigated.

Conclusion

MR based metabolic profiles of non-metastatic breast tumor tissue reflected changes in all patient groups as an effect of chemotherapy. Metabolic profiles discriminated pNRs from pMRD patients after neoadjuvant chemotherapy, which may complement other molecular assays for the elucidation of the underlying mechanisms affecting pathological response. Although metabolic differences based on

bevacizumab administration were not prominent, glutathione was identified to be possibly affected by the antiangiogenic drug.

Abbreviations

Ala: alanine; Asc: ascorbate; ATP: adenosine triphosphate; Cho: choline; Cr: creatine; CV: cross validation; ER: estrogen receptor; FDR: false discovery rate; FEC: 5-fluorouracil-epirubicin-cyclophosphamide; Glc: glucose; Glu: glutamate; Gly: glycine; GPC: glycerophosphocholine; GR: good response; GSH: glutathione; HER2: human epidermal growth factor receptor 2; HIF: hypoxia-inducible factor; HR MAS MRS: high resolution magic angle spinning magnetic resonance spectroscopy; IL-8: interleukin 8; IR: intermediate response; Lac: lactate; LMM: linear mixed-effects model; LV: latent variable; MICE: multiple imputation by chained equations; MR: magnetic resonance; MRI: magnetic resonance imaging; NR: no response; OPLS: orthogonal partial least squares; OS: overall survival; PAM50: prediction analysis of microarrays 50; PC: principal component; PCA: principal component analysis; PCh: phosphocholine; pCR: pathological complete response; PFS: progression-free survival; PLS-DA: partial least squares-discriminant analysis; pMRD: pathological minimal residual disease; pNR: pathological non-responder; PQN: probabilistic quotient normalization; q-q: quantile-quantile; RMSE: root mean square error; ROS: reactive oxygen species; R^2: coefficient of determination; SDH: succinate dehydrogenase; Succ: succinate; Tau: taurine; TCA: tricarboxylic acid; TP: time point; VEGF: vascular endothelial growth factor.

Authors' contributions

LRE, THH, GFG, RV, JE, LSP, GP, LMCB, ALBD, OE, and TFB participated in the design of the study. ALBD, OE, and TFB conceived the study. LRE, THH, GFG, RV, JE, GP, LMCB, ALBD, OE, and TFB interpreted the data. LRE performed the HR MAS MRS acquisition, statistical analysis, and drafted the manuscript. LSP, SL, EB, OG, ALBD, OE, and TFB participated in acquisition of the data. All authors have read and helped to revise the manuscript. The final manuscript is approved by all the authors.

Acknowledgements

The authors would like to thank Øyvind Salvesen for useful discussions regarding linear mixed-effects models and Santosh Lamichhane for technical support during HR MAS MRS acquisition. The HR MAS MRS analysis was performed at the MR Core Facility, Norwegian University of Science and Technology (NTNU), which is funded by the Faculty of Medicine at NTNU and Central Norway Regional Health Authority.

(1) The Research Council of Norway, Imaging the breast cancer metabolome, Project no 221879

(2) The Pink Ribbon Movement and Norwegian Breast Cancer Society
(3) K. G. Jebsen Center for Breast Cancer Research
(4) Roche Norway
(5) Sanofi-Aventis Norway

The funders had no role in study design, data collection and analysis, decision to publish, or preparation of the manuscript.

Competing interests

The NeoAva study was co-sponsored by Roche Norway and Sanofi-Aventis Norway. Oslo University Hospital is the main sponsor for the NeoAva study.

Compliance with ethical requirement

The study was approved for all centers involved by the Regional Ethics Committee (Approval number S-08354a) and the Norwegian Medical Agency. All procedures performed in studies involving human participants were in accordance with the Declaration of Helsinki, International Conference on Harmony/Good Clinical practice. Informed written consent was obtained from all patients.

References

Aboagye, E. O., & Bhujwalla, Z. M. (1999). Malignant Transformation Alters Membrane Choline Phospholipid Metabolism of Human Mammary Epithelial Cells. *Cancer Research, 59*(1), 80-84.

American Cancer Society (2011). Global Cancer Facts & Figures 2nd Edition. Atlanta: American Cancer Society.

Bathen, T. F., Sitter, B., Sjøbakk, T. E., Tessem, M.-B., & Gribbestad, I. S. (2010). Magnetic Resonance Metabolomics of Intact Tissue: A Biotechnological Tool in Cancer Diagnostics and Treatment Evaluation. *Cancer Research, 70*(17), 6692-6696, doi:10.1158/0008-5472.can-10-0437.

Bear, H. D., Tang, G., Rastogi, P., Geyer Jr, C. E., Liu, Q., Robidoux, A., et al. (2015). Neoadjuvant plus adjuvant bevacizumab in early breast cancer (NSABP B-40 [NRG Oncology]): secondary outcomes of a phase 3, randomised controlled trial. *The Lancet Oncology, 16*(9), 1037-1048, doi:http://dx.doi.org/10.1016/S1470-2045(15)00041-8.

Borgan, E., Sitter, B., Lingjærde, O. C., Johnsen, H., Lundgren, S., Bathen, T. F., et al. (2010). Merging transcriptomics and metabolomics–advances in breast cancer profiling. *BMC Cancer, 10*, doi:10.1186/1471-2407-10-628.

Cao, M. D., Giskeodegard, G. F., Bathen, T. F., Sitter, B., Bofin, A., Lonning, P. E., et al. (2012). Prognostic value of metabolic response in breast cancer patients receiving neoadjuvant chemotherapy. *BMC Cancer, 12*, doi:10.1186/1471-2407-12-39.

Cao, M. D., Sitter, B., Bathen, T. F., Bofin, A., Lonning, P. E., Lundgren, S., et al. (2011). Predicting long-term survival and treatment response in breast cancer patients receiving neoadjuvant chemotherapy by MR metabolic profiling. *NMR in Biomedicine, 25*, doi:10.1002/nbm.1762.

Dieterle, F., Ross, A., Schlotterbeck, G., & Senn, H. (2006). Probabilistic Quotient Normalization as Robust Method to Account for Dilution of Complex Biological Mixtures. Application in 1H NMR Metabonomics. *Analytical Chemistry, 78*(13), 4281-4290, doi:10.1021/ac051632c.

Eigenvector Research (2013). Orthogonalizepls. http://wiki.eigenvector.com/index.php?title=Orthogonalizepls. Accessed August 2015.
Fack, F., Espedal, H., Keunen, O., Golebiewska, A., Obad, N., Harter, P., et al. (2015). Bevacizumab treatment induces metabolic adaptation toward anaerobic metabolism in glioblastomas. *Acta Neuropathologica, 129*(1), 115-131, doi:10.1007/s00401-014-1352-5.
Ferlay, J., Soerjomataram, I., Ervik, M., Dikshit, R., Eser, S., Mathers, C., et al. (2013). GLOBOCAN 2012 v1.0, Cancer Incidence and Mortality Worldwide: IARC CancerBase No. 11. http://globocan.iarc.fr. Accessed July 21 2015.
Feron, O. (2009). Pyruvate into lactate and back: From the Warburg effect to symbiotic energy fuel exchange in cancer cells. *Radiotherapy and Oncology, 92*(3), 329-333, doi:http://dx.doi.org/10.1016/j.radonc.2009.06.025.
Ferrara, N., Hillan, K. J., Gerber, H.-P., & Novotny, W. (2004). Discovery and development of bevacizumab, an anti-VEGF antibody for treating cancer. [10.1038/nrd1381]. *Nature Reviews Drug Discovery, 3*(5), 391-400.
Franco, R., & Cidlowski, J. A. (2009). Apoptosis and glutathione: beyond an antioxidant. *Cell Death & Differentiation, 16*(10), 1303-1314, doi:http://www.nature.com/cdd/journal/v16/n10/suppinfo/cdd2009107s1.html.
Gibellini, F., & Smith, T. K. (2010). The Kennedy pathway—De novo synthesis of phosphatidylethanolamine and phosphatidylcholine. *IUBMB Life, 62*(6), 414-428, doi:10.1002/iub.337.
Giordano, S. H., Buzdar, A. U., Smith, T. L., Kau, S.-W., Yang, Y., & Hortobagyi, G. N. (2004). Is breast cancer survival improving? *Cancer, 100*(1), 44-52, doi:10.1002/cncr.11859.
Giskeødegård, G., Cao, M., & Bathen, T. (2015). High-Resolution Magic-Angle-Spinning NMR Spectroscopy of Intact Tissue. In J. T. Bjerrum (Ed.), *Metabonomics* (Vol. 1277, pp. 37-50, Methods in Molecular Biology): Springer New York.
Giskeødegård, G. F., Grinde, M. T., Sitter, B., Axelson, D. E., Lundgren, S., Fjøsne, H. E., et al. (2010). Multivariate Modeling and Prediction of Breast Cancer Prognostic Factors Using MR Metabolomics. *Journal of Proteome Research, 9*(2), 972-979, doi:10.1021/pr9008783.
Giskeødegård, G. F., Lundgren, S., Sitter, B., Fjøsne, H. E., Postma, G., Buydens, L. M. C., et al. (2012). Lactate and glycine—potential MR biomarkers of prognosis in estrogen receptor-positive breast cancers. *NMR in Biomedicine, 25*(11), 1271-1279, doi:10.1002/nbm.2798.
Glunde, K., Bhujwalla, Z. M., & Ronen, S. M. (2011). Choline metabolism in malignant transformation. [10.1038/nrc3162]. *Nature Reviews Cancer, 11*(12), 835-848.
Grinde, M. T., Skrbo, N., Moestue, S. A., Rødland, E. A., Borgan, E., Kristian, A., et al. (2014). Interplay of choline metabolites and genes in patient-derived breast cancer xenografts. *Breast Cancer Research, 16*, R5, doi:10.1186/bcr3597.
Gyanchandani, R., Sano, D., Ortega Alves, M. V., Klein, J. D., Knapick, B. A., Oh, S., et al. (2013). Interleukin-8 as a modulator of response to bevacizumab in preclinical models of head and neck squamous cell carcinoma. *Oral Oncology, 49*(8), 761-770, doi:http://dx.doi.org/10.1016/j.oraloncology.2013.03.452.
Hanahan, D., & Weinberg, R. A. (2000). The Hallmarks of Cancer. *Cell, 100*(1), 57-70, doi:http://dx.doi.org/10.1016/S0092-8674(00)81683-9.
Hanahan, D., & Weinberg, Robert A. (2011). Hallmarks of Cancer: The Next Generation. *Cell, 144*(5), 646-674, doi:http://dx.doi.org/10.1016/j.cell.2011.02.013.
Haukaas, T. H., Euceda, L. R., Giskeødegård, G. F., Lamichhane, S., Krohn, M., Jernström, S., et al. (2016). Metabolic clusters of breast cancer in relation to gene- and protein expression subtypes. [journal article]. *Cancer & Metabolism, 4*(1), 12, doi:10.1186/s40170-016-0152-x.
Hensley, C. T., Wasti, A. T., & DeBerardinis, R. J. (2013). Glutamine and cancer: cell biology, physiology, and clinical opportunities. *The Journal of Clinical Investigation, 123*(9), 3678-3684, doi:10.1172/JCI69600.
Huang, C., & Freter, C. (2015). Lipid Metabolism, Apoptosis and Cancer Therapy. *International Journal of Molecular Sciences, 16*(1), 924.
King, A., Selak, M. A., & Gottlieb, E. (2006). Succinate dehydrogenase and fumarate hydratase: linking mitochondrial dysfunction and cancer. *Oncogene, 25*(34), 4675-4682.

Malmgren, J. A., Parikh, J., Atwood, M. K., & Kaplan, H. G. (2014). Improved Prognosis of Women Aged 75 and Older with Mammography-detected Breast Cancer. *Radiology, 273*(3), 686-694, doi:doi:10.1148/radiol.14140209.

Miller, E., Lee, H., Lulla, A., Hernandez, L., Gokare, P., & Lim, B. (2014). Current treatment of early breast cancer: adjuvant and neoadjuvant therapy [v1; ref status: indexed, *http://f1000r.es/3l2*] (Vol. 3, Vol. 198): F1000Research.

Miller, K., Wang, M., Gralow, J., Dickler, M., Cobleigh, M., Perez, E. A., et al. (2007). Paclitaxel plus Bevacizumab versus Paclitaxel Alone for Metastatic Breast Cancer. *New England Journal of Medicine, 357*(26), 2666-2676, doi:doi:10.1056/NEJMoa072113.

Moestue, S., Sitter, B., Bathen, T. F., Tessem, M.-B., & Gribbestad, I. S. (2011). HR MAS MR spectroscopy in metabolic characterization of cancer. *Current Topics in Medicinal Chemistry, 11*(1), 2-26.

Moestue, S. A., Giskeødegård, G. F., Cao, M. D., Bathen, T. F., & Gribbestad, I. S. (2012). Glycerophosphocholine (GPC) is a poorly understood biomarker in breast cancer. *Proceedings of the National Academy of Sciences, 109*(38), E2506, doi:10.1073/pnas.1208226109.

Ng, C. K., Pemberton, H. N., & Reis-Filho, J. S. (2012). Breast cancer intratumor genetic heterogeneity: causes and implications. *Expert Review of Anticancer Therapy, 12*(8), 1021-1032, doi:doi:10.1586/era.12.85.

Parker, J. S., Mullins, M., Cheang, M. C. U., Leung, S., Voduc, D., Vickery, T., et al. (2009). Supervised Risk Predictor of Breast Cancer Based on Intrinsic Subtypes. *Journal of Clinical Oncology, 27*(8), 1160-1167, doi:10.1200/jco.2008.18.1370.

Perou, C. M., Sorlie, T., Eisen, M. B., van de Rijn, M., Jeffrey, S. S., Rees, C. A., et al. (2000). Molecular portraits of human breast tumours. [10.1038/35021093]. *Nature, 406*(6797), 747-752, doi:http://www.nature.com/nature/journal/v406/n6797/suppinfo/406747a0_S1.html.

Pinheiro, J., Bates, D., DebRoy, S., Sarkar, D., & R Core Team (2014) (2014). nlme: Linear and Nonlinear Mixed Effects Models. R package version 3.1-117, URL: http://CRAN.R-project.org/package=nlme.

Pinheiro, J. C., & Bates, D. M. (2000). Linear Mixed-Effects Models: Basic Concepts and Examples. In *Mixed-Effects Models in S and S-PLUS* (pp. 3-56, Statistics and Computing). New York, NY, USA: Springer New York.

R Core Team (2014). R: A language and environment for statistical computing. http://www.R-project.org/.Viena, Austria. URL http://www.R-project.org/: R Foundation for Statistical Computing.

Rubin, D. B. (1987). *Mulitiple Imputation for Nonresponse in Surveys*. New York, USA: John Wiley & Sons.

Saraswathy, S., Crawford, F., Lamborn, K., Pirzkall, A., Chang, S., Cha, S., et al. (2009). Evaluation of MR markers that predict survival in patients with newly diagnosed GBM prior to adjuvant therapy. *Journal of Neuro-Oncology, 91*(1), 69-81, doi:10.1007/s11060-008-9685-3.

Selak, M. A., Armour, S. M., MacKenzie, E. D., Boulahbel, H., Watson, D. G., Mansfield, K. D., et al. (2005). Succinate links TCA cycle dysfunction to oncogenesis by inhibiting HIF-α prolyl hydroxylase. *Cancer Cell, 7*(1), 77-85, doi:http://dx.doi.org/10.1016/j.ccr.2004.11.022.

Semenza, G. L. (2008). Tumor metabolism: cancer cells give and take lactate. *The Journal of Clinical Investigation, 118*(12), 3835-3837, doi:10.1172/JCI37373.

Sitter, B., Sonnewald, U., Spraul, M., Fjösne, H. E., & Gribbestad, I. S. (2002). High-resolution magic angle spinning MRS of breast cancer tissue. *NMR in Biomedicine, 15*(5), 327-337, doi:10.1002/nbm.775.

Sørlie, T., Tibshirani, R., Parker, J., Hastie, T., Marron, J. S., Nobel, A., et al. (2003). Repeated observation of breast tumor subtypes in independent gene expression data sets. *Proceedings of the National Academy of Sciences, 100*(14), 8418-8423, doi:10.1073/pnas.0932692100.

van Buuren, S., & Groothuis-Oudshoorn, K. (2011). mice: Multivariate Imputation by Chained Equations in R. *Journal of Statistical Software, 45*(3), 1-67.

van der Hage, J. A., van de Velde, C. J. H., Julien, J.-P., Tubiana-Hulin, M., Vandervelden, C., Duchateau, L., et al. (2001). Preoperative Chemotherapy in Primary Operable Breast Cancer: Results From the European Organization for Research and Treatment of Cancer Trial 10902. *Journal of Clinical Oncology, 19*(22), 4224-4237.

Vander Heiden, M. G., Cantley, L. C., & Thompson, C. B. (2009). Understanding the Warburg Effect: The Metabolic Requirements of Cell Proliferation. *Science, 324*(5930), 1029-1033, doi:10.1126/science.1160809.

Végran, F., Boidot, R., Michiels, C., Sonveaux, P., & Feron, O. (2011). Lactate Influx through the Endothelial Cell Monocarboxylate Transporter MCT1 Supports an NF-κB/IL-8 Pathway that Drives Tumor Angiogenesis. *Cancer Research, 71*(7), 2550-2560, doi:10.1158/0008-5472.can-10-2828.

Walenta, S., & Mueller-Klieser, W. F. (2004). Lactate: mirror and motor of tumor malignancy. *Seminars in Radiation Oncology, 14*(3), 267-274, doi:http://dx.doi.org/10.1016/j.semradonc.2004.04.004.

Walenta, S., Wetterling, M., Lehrke, M., Schwickert, G., Sundfør, K., Rofstad, E. K., et al. (2000). High Lactate Levels Predict Likelihood of Metastases, Tumor Recurrence, and Restricted Patient Survival in Human Cervical Cancers. *Cancer Research, 60*(4), 916-921.

Westerhuis, J., Hoefsloot, H. J., Smit, S., Vis, D., Smilde, A., van Velzen, E. J., et al. (2008). Assessment of PLSDA cross validation. *Metabolomics, 4*(1), 81-89, doi:10.1007/s11306-007-0099-6.

Wold, S., Esbensen, K., & Geladi, P. (1987). Principal Component Analysis. *Chemometrics and Intelligent Laboratory Systems, 2*, 37-52.

Wold, S., Sjöström, M., & Eriksson, L. (2001). PLS-regression: a basic tool of chemometrics. *Chemometrics and Intelligent Laboratory Systems, 58*(2), 109-130, doi:http://dx.doi.org/10.1016/S0169-7439(01)00155-1.

Xie, J., Wu, H., Dai, C., Pan, Q., Ding, Z., Hu, D., et al. (2014). Beyond Warburg effect - dual metabolic nature of cancer cells. [Article]. *Scientific Reports, 4*, doi:10.1038/srep04927 http://www.nature.com/srep/2014/140513/srep04927/abs/srep04927.html#supplementary-information.

Tables

Table 1. Patient and tumor characteristics.

		Total	Bevacizumab-treated	Chemotherapy Only
Number of patients		122	60	62
Mean age (range)	years	49.0 (25 – 70)	49.6 (27-70)	48.4 (25-68)
Therapy Response				
Pathological complete response (pCR)	pCR	20	13	7
	No pCR	102	47	55
Pathological minimal residual disease (pMRD)	pMRD	44	24	20
	Pathological non-responder (pNR)	78	36	42
Response ratio	Good response (GR)	31	18	13
	Intermediate response (IR)	69	32	37
	No response (NR)	22	10	12
Histology	Ductal	98	47	51
	Lobular	21	12	9
	Other	3	1	2
T status at TP1	T1	0	0	0
	T2	36	17	19
	T3	74	37	37
	T4	11	5	6
	NA	1	1	0
T status at TP3	T1	49	21	28
	T2	36	20	16
	T3	14	5	9
	T4	0	0	0
	NA	23	14	9
Node status at TP3	N0	45	23	22
	N1	30	14	16
	N2	14	5	9
	N3	4	0	4
	NA	29	18	11
ER status	+	101	48	53
	-	21	12	9
PgR status	+	70	32	38
	-	51	27	24
	NA	1	1	0

NA: not available

Table 2. LMM results for the fixed effects of *time*, *pMRD response*, and *bevacizumab*.

	TP2 vs TP1	TP3 vs TP2	pMRD vs pNR	Bev-treated vs Chemo-only	Significant Interactions[#]
Glc	0.130* (0.065)	0.309** (0.064)	-0.155 (0.078)	0.096 (0.055)	*Time* × *Response*
Asc	-0.036* (0.015)	-0.107** (0.014)	-0.016 (0.017)	0.005 (0.017)	None
Lac	0.173** (0.050)	0.398** (0.048)	0.157** (0.049)	0.053 (0.047)	None
Tyr	-0.047* (0.023)	-0.121** (0.022)	0.052* (0.026)	-0.023 (0.016)	*Time* × *Response*
mI	0.050** (0.016)	0.035** (0.015)	-0.014 (0.021)	-0.003 (0.020)	None
Gly	-0.029 (0.017)	0.004 (0.016)	0.011 (0.021)	0.018 (0.020)	None
Tau	<0.001 (0.021)	0.042* (0.021)	-0.059* (0.026)	0.014 (0.018)	*Time* × *Response*
GPC	-0.032 (0.018)	-0.057** (0.017)	-0.001 (0.022)	-0.022 (0.021)	None
PCh	-0.061** (0.023)	-0.101** (0.023)	0.057 (0.029)	-0.024 (0.021)	*Time* × *Response*
Cho	-0.055** (0.018)	-0.043** (0.018)	0.051* (0.022)	-0.034* (0.015)	*Time* × *Response*
Cr	-0.015 (0.017)	-0.048** (0.016)	-0.034 (0.018)	0.007 (0.017)	None
GSH	0.022 (0.030)	-0.045 (0.030)	0.044 (0.029)	0.057* (0.029)	*Time* × *Response;* *Time* × *Bevacizumab*
Gln	0.021 (0.022)	0.119** (0.021)	-0.011 (0.026)	-0.007 (0.025)	None
Succ	-0.035 (0.037)	0.035 (0.036)	0.048 (0.042)	-0.032 (0.027)	*Time* × *Response*
Glu	0.018 (0.021)	0.014 (0.020)	0.064* (0.025)	0.045 (0.024)	None
Ala	0.042 (0.029)	0.096** (0.028)	-0.016 (0.028)	0.039 (0.026)	None

Metabolite increase (positive estimate) or decrease (negative estimate) is shown for TP2, TP3, pMRD, and bevacizumab-treated patients in relation to TP1,TP2, pNR, and chemotherapy-only patients, respectively. Standard errors are shown in parenthesis. * and ** indicate significance ($p \leq 0.05$) before and after multiple testing correction, respectively.

[#]Final LMMs shown here were built including significant interaction terms, but interaction results are presented separately in Table 3.

pMRD: pathological minimal residual disease; pNR: pathological non-responder; Bev-treated: Bevacizumab-treated; Chemo-only: Chemotherapy-only; Glc: glucose; Asc: ascorbate; Lac: lactate; Tyr: tyrosine; mI: myo-inositol; Gly: glycine; Tau: taurine; GPC: glycerophosphocholine; PCh: phosphoscholine; Cho: choline; Cr: creatine; GSH: glutathione; Gln: glutamine; Succ: succinate; Glu: glutamate; Ala: alanine.

Figure Legends

Fig. 1. PCA including all samples. (A) The scores plot shows a trend in the direction of the arrow with increasing time point. (B) PQN-normalized mean spectra at each time point. Gray bars indicate removed spectral regions. (C) The normal-like gene expression subtype is most clearly separated from the rest in the scores plot, showing a similar distribution as TP3 in A. (D) The loadings plot indicates higher phosphocholine, glycerophosphocholine, and taurine at TP1 and increasing glucose and lipids with increasing time of treatment and in normal-like samples. Loadings are colored according to LV1. LumA=luminal A; LumB=luminal B; Norm-like=normal-like; NA=not available; Glc=glucose; Asc=ascorbate; Lac=lactate; mI=myo-inositol; Tyr=tyrosine; Cr=creatine; Gly=glycine; Tau=taurine; GPC=glycerophosphocholine; PCh=phosphoscholine; Cho=choline; GSH=glutathione; Gln=glutamine; Succ=succinate; Glu=glutamate; Ala=alanine.

Fig. 2. PLS-DA scores (A) and loadings (B) plots of pathological complete responders (pCR+) vs patients with no pathological complete response (pCR-) at TP3, and PLS-DA scores (C) and loadings (D) plots of pathological minimal residual disease patients (pMRD) vs pathological non-responders (pNRs) at TP3. Both pCR+ (A) and pMRD (C) display lower scores along LV1 than pCR- and pNRs, respectively. Loadings show pCR+ (B) and pMRD (D) having higher glucose and lactate compared to pCR- and pNRs, respectively, and lower levels of the choline containing metabolites, creatine, glycine, taurine, succinate, and alanine. Loadings are colored according to LV1. Glc=glucose; Lac=lactate; Lip=lipids; Cr=creatine; Gly=glycine; Tau=taurine; GPC=glycerophosphocholine; PCh=phosphoscholine; Cho=choline; Succ=succinate; Ala=alanine.

Fig. 3. PLS-DA scores and loadings plots of good response (GR) vs no response (NR) patient groups at TP1 (A-B) and TP3 (C-D). (A) At TP1, the GR group displays lower scores along LV1 than the NR group, with loadings showing the former group having lower glucose, and higher levels of lactate, taurine, the choline containing metabolites, glutathione, and succinate, among others (B). (C) At TP3, the GR group also displays lower scores along LV1, but the loading profile (D) is inverted when compared to TP1, indicating a metabolic switch related to tumor reduction with treatment time. Loadings are colored according to LV1. Glc=glucose; Asc=ascorbate; Lac=lactate; Tyr=tyrosine; Cr=creatine; Gly=glycine; Tau=taurine; GPC=glycerophosphocholine; PCh=phosphoscholine; Cho=choline; GSH=glutathione; Succ=succinate; Glu=glutamate; Ala=alanine.

Fig. 4. Illustration of treatment effect and differences between responders and non-responders. Cancer-relevant pathways shown include glycolysis (brown), tricarboxylic acid (TCA) cycle (black), choline phospholipid metabolism (orange), glutaminolysis (gray), and glutathione biosynthesis (blue),

with altered metabolites and related enzymes marked in red and purple, respectively . General trends in metabolite levels with increasing treatment time (Tx) and differences in pathological minimal residual disease patients compared to pathological non-responders (pMRD) and in the response ratio group of good response compared to the no response group (GR) at each time point (TP) indicated with arrows are shown in red boxes. TCA cycle reactions that are recruited by glutaminolysis are marked ◊.

Supplementary Material

Supplementary Material 1: Supplementary methods and references

SupplementaryInformation.pdf

Information on supplementary methods.

Supplementary Material 2: Supplementary Figures

SupplementaryFigures.pdf

Supplementary Figures S1-S3.

Supplementary Material 3: Supplementary Table 2

SupplementaryTable2.xlsx

Supplementary Table 2.

Supplementary Material 4: Supplementary Tables 3-8

SupplementaryTables.pdf

Supplementary Tables 3-8.

Figures

Figure 1:

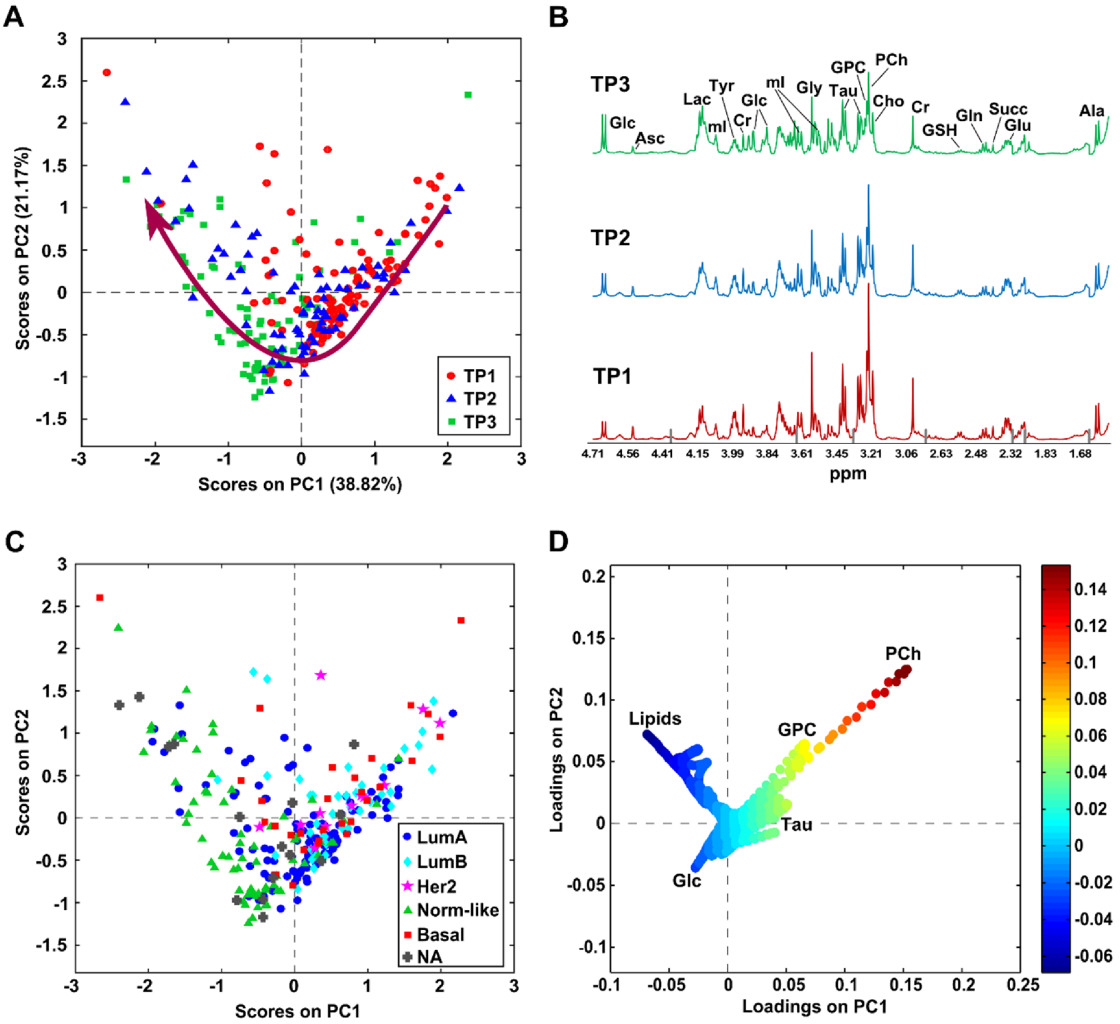

Figure 2:

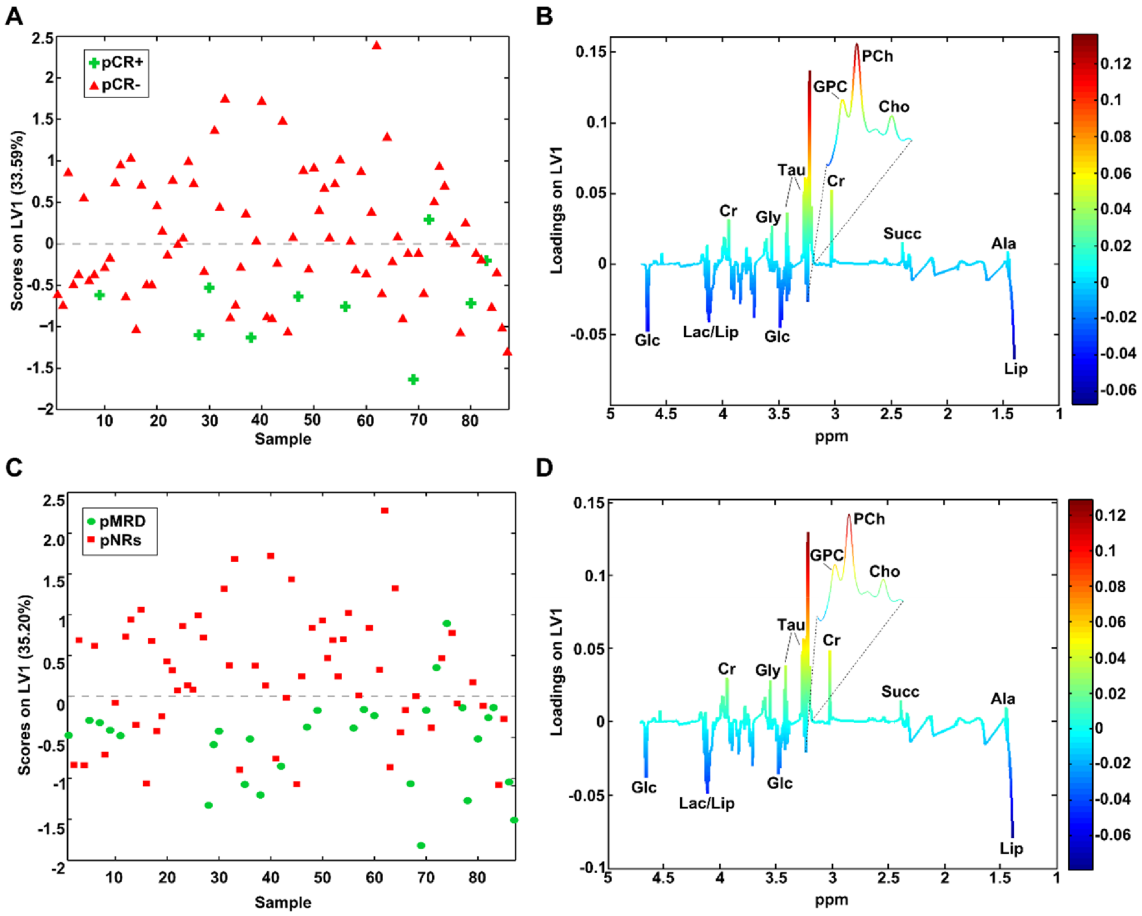
A
pCR+
pCR-
Scores on LV1 (33.59%)
Sample
B
Loadings on LV1
PCh
GPC
Cho
Tau
Cr
Cr
Gly
Succ
Ala
Glc
Lac/Lip
Glc
Lip
ppm
C
pMRD
pNRs
Scores on LV1 (35.20%)
Sample
D
Loadings on LV1
PCh
GPC
Cho
Tau
Cr
Cr
Gly
Succ
Ala
Glc
Lac/Lip
Glc
Lip
ppm

Figure 3:

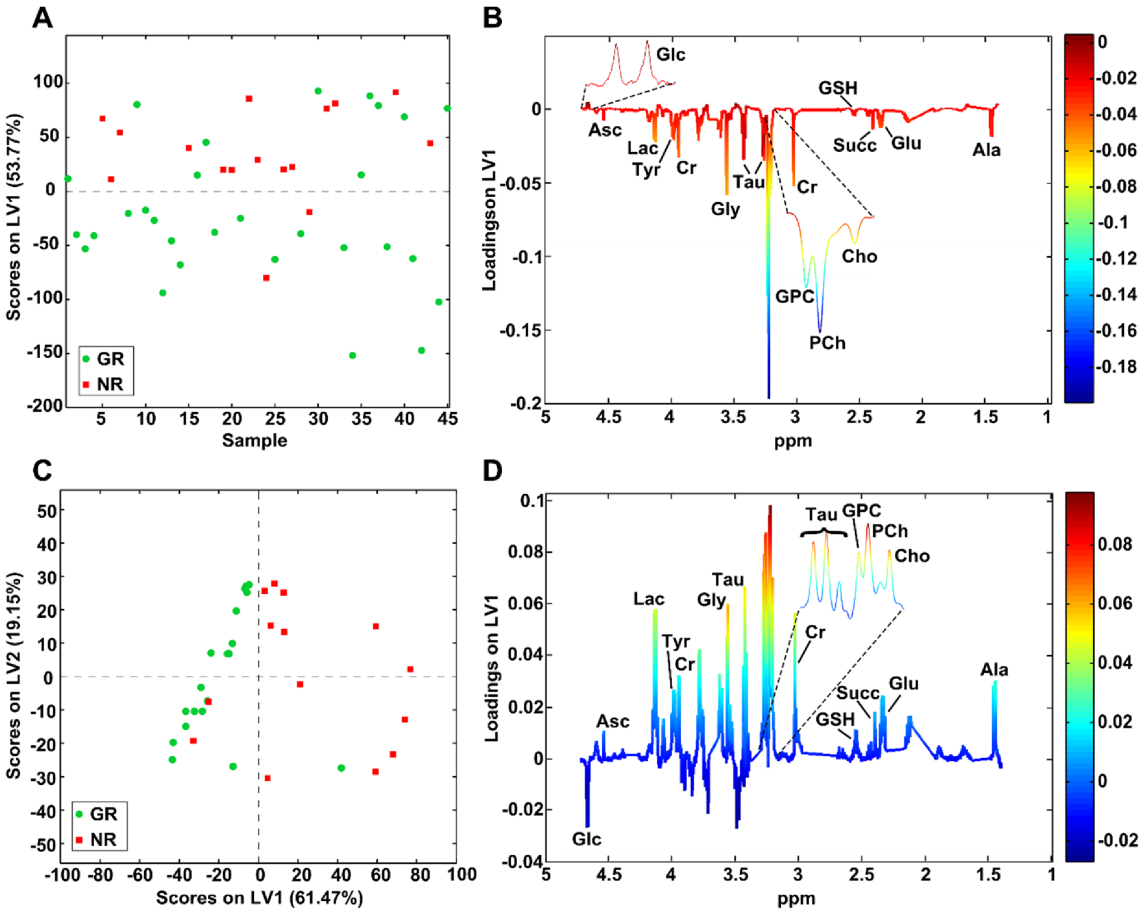
A
Scores on LV1 (53.77%)
Sample
GR
NR
B
Loadingson LV1
ppm
Glc
Asc
Lac
Tyr
Cr
Gly
Tau
GSH
Succ
Glu
Ala
Cho
GPC
PCh
C
Scores on LV2 (19.15%)
Scores on LV1 (61.47%)
GR
NR
D
Loadings on LV1
ppm
Tau
GPC
PCh
Cho
Lac
Gly
Tyr
Cr
Asc
Succ
Glu
GSH
Ala
Glc

Figure 4:

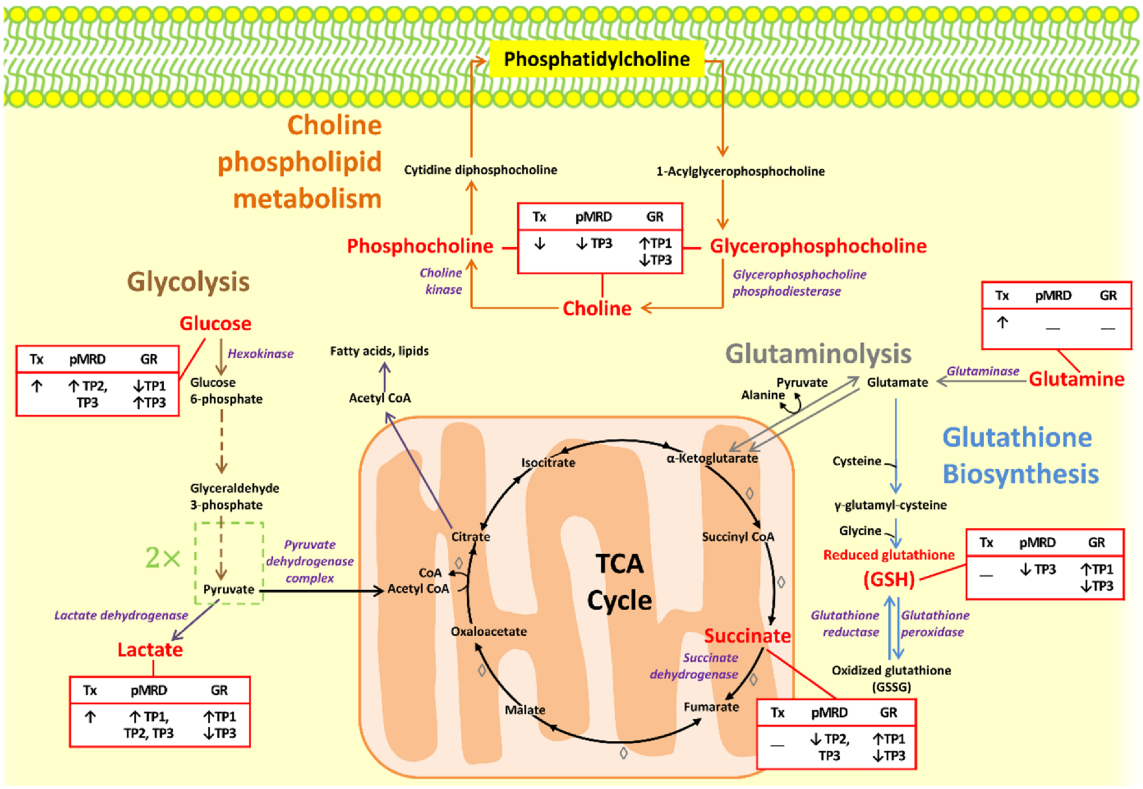
Phosphatidylcholine
Choline phospholipid metabolism
Cytidine diphosphocholine
1-Acylglycerophosphocholine
Tx pMRD GR
↓ ↓TP3 ↑TP1 ↓TP3
Phosphocholine
Glycerophosphocholine
Choline kinase
Glycerophosphocholine phosphodiesterase
Choline
Glycolysis
Glucose
Tx pMRD GR
↑ ↑TP2, TP3 ↓TP1 ↑TP3
Hexokinase
Glucose 6-phosphate
Glyceraldehyde 3-phosphate
2×
Pyruvate dehydrogenase complex
Pyruvate
Lactate dehydrogenase
Lactate
Tx pMRD GR
↑ ↑TP1, TP2, TP3 ↑TP1 ↓TP3
Fatty acids, lipids
Acetyl CoA
Isocitrate
α-Ketoglutarate
Citrate
Succinyl CoA
CoA
Acetyl CoA
TCA Cycle
Oxaloacetate
Succinate
Succinate dehydrogenase
Malate
Fumarate
Tx pMRD GR
— ↓ TP2, TP3 ↑TP1 ↓TP3
Glutaminolysis
Tx pMRD GR
↑ — —
Glutaminase
Glutamine
Pyruvate
Alanine
Glutamate
Glutathione Biosynthesis
Cysteine
γ-glutamyl-cysteine
Glycine
Reduced glutathione
(GSH)
Tx pMRD GR
— ↓ TP3 ↑TP1 ↓TP3
Glutathione reductase
Glutathione peroxidase
Oxidized glutathione (GSSG)